

Quantitative Analysis of Synaptic Ultrastructure in The Mouse Cerebellum by Focused Ion Beam-Scanning Electron Microscopy: A novel Method for Structural Analysis

Ruwaida Elhanbaly^{1*}, Yugo Fukazawa^{2,3,4}

¹Department of Anatomy and Embryology, Faculty of Veterinary Medicine, Assiut University, Assiut 71515, Egypt.

²Division of Brain Structure and Function, Faculty of Medical Sciences, University of Fukui, Fukui, Japan.

³Research Center for Child Mental Development, Faculty of Medical Sciences, University of Fukui, Fukui, Japan.

⁴Life Science Innovation Center, University of Fukui, Fukui, Japan.

*Correspondence

Ruwaida Elhanbaly

Department of Anatomy and Embryology, Faculty of Veterinary Medicine, Assiut University, Assiut 71515, Egypt.

E-mail address: Ruwaida@aun.edu.eg

Abstract

The present study was carried out to investigate the synaptic ultrastructure of the mouse cerebellum using focused ion beam scanning electron microscopy (FIB-SEM). The experiment were performed using seven weeks old wild type mice. In the present work, we used a newly established morphological investigation method of axospinous synapses (FIB-SEM). This method enables fully automated acquisition of serial ultrastructural data at a spatial resolution of 10 nm in z-axis without the ultrastructure distortions. FIB-SEM enabled easily identification of axospinous synapses in the mouse cerebellum where individual synaptic ultra-structure can be easily identified and measured. The results indicated that, the cerebellum axospinous synapses have presynaptic and postsynaptic compartment. The presynaptic compartment consists of the presynaptic axonal varicosity, synaptic vesicles and mitochondria. The postsynaptic compartment consists of the dendritic spine, postsynaptic density and smooth endoplasmic reticulum and spine apparatus. The volume of presynaptic and postsynaptic compartments was variable. The results indicated a significant positive correlation between presynaptic compartments as well as between postsynaptic compartments. Moreover, this study represented novel correlations between presynaptic and postsynaptic parameters.

KEYWORDS

Neurons, Synapses, plasticity, FIB-SEM

INTRODUCTION

The power of the brain is based upon the extraordinary abilities of nerve cells to communicate with each other at specialized intracellular junctions called synapses (Burns and Augustine, 1995). The key elements required for signal transduction and plasticity in the brain are synapses. In order to understand the functional signal cascades underlying synaptic transmission, a quantitative morphological analysis of the pre- and postsynaptic structures that represent morphological correlations for synaptic transmission is important. Although all synapses are composed of almost the same structural elements, the composition of these elements within a given synapse and the microcircuit in which they are embedded are the deciding factors determining its function (Rollenhagen and Lübke, 2006).

Synapses are considered the primary link between neurons and have both presynaptic and postsynaptic components, separated by the synaptic cleft. The presynaptic part comprises a vesicle-filled axon terminal, with a small number of vesicles fused to or docked near the presynaptic membrane, and a very thin layer of electron-dense material immediately adjacent to the synaptic cleft. The postsynaptic part consists of an electron-dense plate called the postsynaptic density (Harris and Weinberg, 2012).

Many studies have tried to get simple and accurate methods for estimating the distribution, number and size of axospinous synapses. Currently, numerous methods are available even though most are based on sampling relatively few single sections. However, serial section reconstruction should be the method of choice when the final goal is for understanding three-dimensional characteristics (Harris *et al.*, 2006). Three-dimensional reconstructions are so important to study the synaptic connectivity and the function and they help unravel the extracomplexity of the nervous system (DeFelipe, 2009). One of the main goals in the neuroscience is to determine the microcircuits that exist in the brain and how they share in functional organization both in health and disease (Harris *et al.*, 2006; Merchan-Perez *et al.*, 2009).

In order to understand the mechanisms underlying higher order functions and their impairments of the brain, not only information about neuronal networks embedded in the brain, but also information about structural diversity of individual contacts of neurons (synapses) at individual connections is necessary. Therefore, new approaches by which functional property of individual synapses and identity of the synaptic connection could be extrapolated from structural properties of a given synapse may provide dynamic picture of brain networks and facilitate understanding about the computation mechanisms of the brain.

Synaptic transmission and plasticity are crucial for all aspects of nervous system function and critical for proper development of the central nervous system. Normal synaptic transmission depends on the proper localization and arrangement of specific proteins on both sides of the synapse. So, pathological synapse development and/or function almost certainly contribute to many neuropsychiatric disorders (Harris *et al.*, 1992).

Quantitative analysis of axospinous synapses appears to be of essential importance, not only because it is essential to know and understand the structure of the basic types of cerebellar synapses but also, because the exact morphologies of cerebellar synapses could be intricately related to their function (Arellano *et al.* 2007).

Serial section transmission electron microscopy (ssTEM) is a well-settled technique for obtaining three-dimensional data from ultrathin sections of brain tissue, however the major restriction is that obtaining long series of ultrathin sections is extremely time consuming and difficult, often making it impossible to reconstruct large volumes of tissue. There are some problems must be overcome, including sections loss, different thickness, the recurrent existence of debris or artifacts in sections as well as geometrical disorders. Generally to resolve these problems requires intensive human interaction and accurate training, which impairs these approaches to be widely used (Hoffpauer *et al.*, 2007; Kubota *et al.*, 2009).

The focused ion beam scanning electron microscopy offers the advantages that the process of obtaining serial images is fully automated, eliminating the need for serial sectioning, collection of ultrathin sections and manual acquisition of microphotographs. Moreover, given that the images are taken from the block face, they are almost completely aligned and the completion of alignment can be fully automated (Merchan-Perez *et al.*, 2009). The 3DEM technique provides accurate detection of distribution and density of subcellular synaptic structures (smooth endoplasmic reticulum, polyribosomes, mitochondria, microtubules and endosomal compartments). So that we apply the 3DEM technique in the mouse cerebellum to show all previously mentioned structures.

MATERIALS AND METHODS

All experiments were conducted in accordance with the regulation of animal research at Fukui University, Japan. The experiments were performed using seven weeks old wild type mice. In the present work, we used a newly established morphological investigation method of axospinous synapses by focused ion beam-scanning electron microscope (FIB-SEM). This method enables fully automated acquisition of serial ultrastructural data at a spatial resolution of 10 nm in z-axis without the ultrastructure distortions.

Sample preparation for focused ion beam scanning electron microscopy (FIB/SEM)

Animal perfusion

The mice (C57BL/6J) were transcidentally perfused through the ascending aorta with saline followed by 0.5 karnovsky fixatives. Then the head was removed using a pair of scissors. The dorsal surface of the skull was peeled away from the brain. The olfactory bulbs and nervous connections along the ventral surface of the brain were severed. The brain was teased gently away from the head and any dura was trimmed. The brain was removed and placed in a vial of fixative (4% paraformaldehyde) containing fluid

at least 10x the volume of the brain itself. The vial was swirled occasionally. The brain was examined under a dissecting microscope to determine its well perfusion. If the surface of the brain appeared well perfused, the cerebellum and the surrounding structures were placed in 0.1 M sodium cacodylate for further processing. Post-fixed area overnight in 4% paraformaldehyde at 4°C. After that, these specimens were washed with phosphate buffered saline by exchanging the media 3 times.

Sections preparation (protocol used for focused ion beam scanning electron microscopy)

After overnight fixation, the specimens were washed three times with phosphate buffer saline. They were sectioned 100 um thick sections in cold 0.1 M phosphate buffer using vibratome. The sections were washed in cold cacodylate buffer containing 2mM calcium chloride for five minute. This step was repeated three times (3x5 minutes).The samples were freely distributed throughout the solution, and not floated to the surface of the well. The tissues were incubated in a solution containing 3% potassium ferrocyanide in 0.2M cacodylate buffer with 4mM calcium chloride was combined with an equal volume of 4% osmium tetroxide and kept on ice for 1 hour. Sections were turned to dark brown colour. Then the sections were washed with ddH₂O at room temperature for 3x5 minutes and placed in filtered thio-cabohdrazide (TCH) for 20 minutes also at room temperature. The sections were washed with ddH₂O for 3x5 minutes and then placed in 2% osmium tetroxide aqueous for 30 minutes at room temperature. The sections were washed with ddH₂O at room temperature for 3x5 minutes after this second exposure to 2% osmium tetroxide. The sections were placed in 1% uranyl acetate (aqueous) and left overnight (18 h) at 4°C. On day 2, the sections were washed with ddH₂O at room temperature for 3x5 minutes and then placed in freshly prepared lead aspartate solution and kept in the oven at 60°C for 75 minutes. They were washed with ddH₂O at room temperature for 3x5 minutes and then they dehydrated using solutions of 50%, 70%, 80%, 90%, 95%, 100% (twice) ethanol for 5 minutes each, then placed in propylene oxide (PO) and left at room temperature for 10 minutes. During this time Durcupan ACM resin is formulated by weight as follow: 11.4 g part A, 10 g part B, 0.3 g part C and 0.05-0.1 (0.07) part D. the resin is mixed thoroughly. Sections were placed in 25%, 50%, 75% Durcupan: Propylene oxide each for 2 h, followed by 100% Durcupan overnight. On day 3, sections were placed into the fresh Durcupan (100%) for 5 h, and then flat embedded between liquid release agent-coated glass slides and placed in a 60°C for 48 h. The cerebellum was then trimmed out of the flat embedded sample, and is glued to a Durcupan block so that one side of the tissue can be exposed using an ultramicrotome. The exposed surface was then glued to a metal rivet (pin) using glue (FIB-SEM) or 2 parts silver epoxy (DK-SEM 1:1 A: B) and left to dry at 60°C for 1 h). The resin of the other side was trimmed away using an ultramicrotome so that this side of the sample is also exposed. The surface was coated with thin layer of carbon (5 nm) by a conventional carbon coater or a BFA060 freeze etching machine (Knott *et al.*, 2011).

Imaging in the FIB/SEM

At low magnification, and using secondary electron imaging (5 kV, 0.5 nAmp), the block was oriented so that the chosen region of cerebellum and the side of the block to be imaged was facing the operator. The block was oriented so that the face to be imaged laid parallel to the milling beam. This meant that electron

beam was oriented at 54 ° to this face. An ion beam current of 5 nAmps at 30 kV was used to remove a narrow band of resin from the front of the region to be imaged. Switched to backscattered imaging mode to view the milled face that overlies the region of interest. The light microscopy reference image and the image of the milled face located in the exact region were used on the block to be milled and imaged. We used a current of 700 pico-Amps, finely milled the region of the block within which the final images would be taken. The milling beam was left to completely mill this image face until no milling artifacts could be seen on the face. A complete mill of the face was checked by observing changes in each subsequent image across the entire field of view. Inadequate milling could also be seen as white streaks or curtains that appear vertically in the image. The microscope was left for at least 2 hours for any thermal changes to dissipate. This reduced the risk that the block face will drift during imaging resulting in misaligned images. The microscope parameters were selected for imaging the face serially. We ensured that the electron beam has a voltage that was low enough to only image a very shallow depth of material in the block face. This should also be much shallower than the thickness of the face to be removed. Typical parameters for imaging were voltages of between 1.2 - 2.0 kV with pixel sizes of between 4 - 20 nm. The pixel dwell time needs to be kept around 10 µsecs so that the total time to mill the face and acquire one image is maintained below 2 minutes. We used shooting magnification at 17500 and the photographing conditions at 1.5 kv, 0.2 to 0.4 Na, dual time 5 µsecs, 6144 x 4096 pixel, Z step = 10 nm.

Data analysis

Image stacks: the dataset contains 759 serial images. TrakEM2 software was used to assemble images for three dimensional reconstruction and analysis.

Image measurement: Volumetric measurements were generated in TrakEM2 software.

The image dimensions of cerebellum was shown in Table 1.

Table 1. Showing the image dimensions of cerebellum.

| Parameters | Cerebellum region |
|-------------------------|-------------------|
| Voxel width | 1.927 |
| Voxel height | 1.927 |
| Voxel depth (nm) | 10 |
| Slice thickness (pixel) | 5.189 |

Measured parameters

The synaptic populations was randomly selected for reconstruction of the entire synaptic contact including presynaptic axonal varicosity (AV), synaptic vesicle (SV), mitochondria (M), postsynaptic dendritic spine (S), postsynaptic density (PSD), smooth endoplasmic reticulum (sER) and the spine apparatus (SA).

Statistical tests

Statistical tests were done by SPSS software. In all cases, data was tested for normality test. If the data sets were normal, parametric tests were used. Otherwise nonparametric tests were used.

RESULTS

The axospinous synapses are excitatory synaptic contacts es-

tablished on dendritic spines. The dendritic spines are tiny protrusions which extend from dendrites of postsynaptic neurons. The axospinous synapses have presynaptic and postsynaptic compartment.

The presynaptic compartment consists of the presynaptic axonal varicosity, synaptic vesicles and mitochondria. The postsynaptic compartment consists of the dendritic spine, postsynaptic density and smooth endoplasmic reticulum and spine apparatus. Focused ion beam scanning electron microscopy enabled easily identification of axospinous synapses in the mouse cerebellum where individual synaptic ultra-structure can be easily identified and measured (Fig. 1).

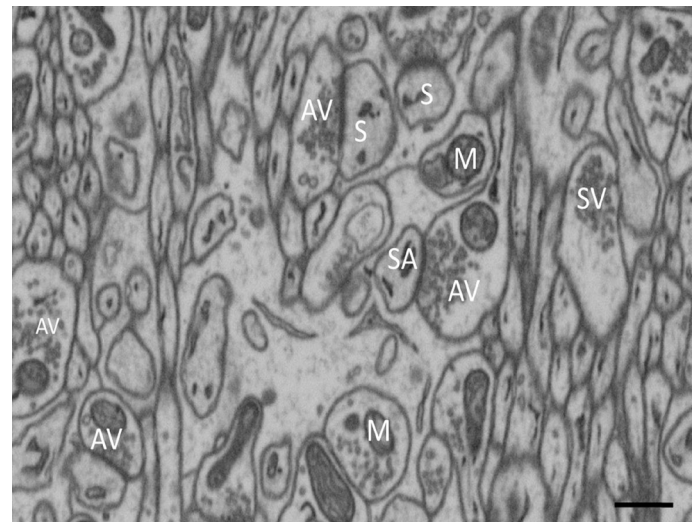


Fig. 1. Panoramic view of the neuropil obtained by FIB/SEM of the mouse cerebellum showing: The high quality of the image. Individual ultrastructural components of cerebellar mouse synapses can be clearly seen in the image. (SV) Synaptic vesicles, (M) Mitochondria and (SA) Spine apparatus. Some axonal varicosities (AV) establish clearly identifiable axospinous synapses with dendritic spines (S) and dendrite (D). Scale bar, 3 µm.

Morphological and morphometrical analysis

Presynaptic compartment

Presynaptic axonal varicosity

Presynaptic varicosities of axospinous synapses were identified by their dimensions and components. The presynaptic varicosities were easily identified by their shape alone; in addition they had vesicles or mitochondria. The axonal varicosities were visualized and examined for their composition of synaptic vesicles and mitochondria; some were small and others large.

The obtained results indicated that most of axonal varicosities had only one spine synapsing with them (single spine bouton SSB). Some varicosities had more than one spine synapsing with them (multispine bouton MSB). These spines shared a contiguous population of synaptic vesicles and often differ from one another in shape (Fig. 2). However there were a significantly greater number of synaptic vesicles in multispine bouton than single spine bouton. The frequency of MSB was 5% from the reconstructed axospinous synapses.

Three-dimensional reconstruction of presynaptic varicosities showed great diversity in size and shape (Fig. 3). The volume of presynaptic varicosity ranged from 0.147-0.881 µm³. The average volume was 0.338 ± 0.0386 µm³ (Table 2).

Synaptic vesicles

Using FIB/SEM with 10 nm Z- step, each synaptic vesicle became easily identified and accurately counted within each pre

Table 2. Summary of measurement results of presynaptic parameters.

| Presynaptic parameters | | cerebellum |
|------------------------|-----------------|-----------------|
| PreV | N | 20 |
| | V (range) | 0.147-0.881 |
| | V (average) ±SE | 0.338±0.0386 |
| SVs | N (range) | 59 -392 |
| | N (average) ±SE | 171.55±19. 5462 |
| Mit. | N | 13 |
| | Nmit/preV | 0.65 |
| | V (range) | 0.017-0.098 |
| | V (average) ±SE | 0.050±0.0072 |
| MSB% | Nmsb/NpreV | (5%)1/20 |

N (Number), V (Volume), SE (Standard Error)

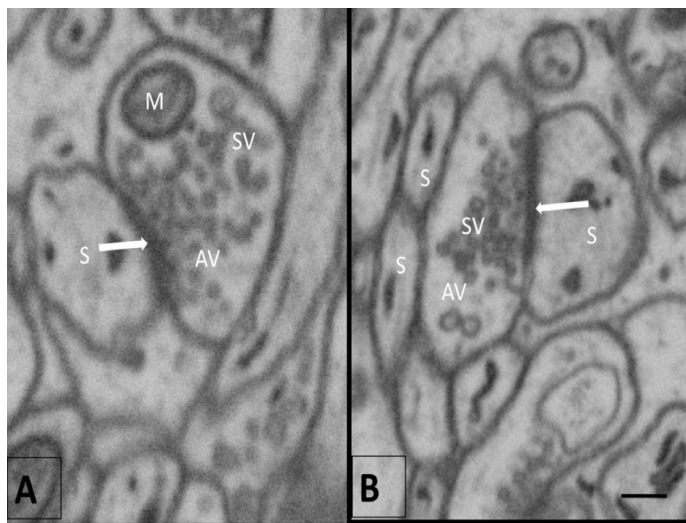


Fig. 2 (A, B). Axospinous synapse from cerebellar purkinje fibers showing: (A) Single spine bouton, The axonal varicosity (AV) is synapsed with single spine (S). (B) Multispine bouton, Axonal varicosity(AV), Synaptic vesicles(SV), Dendritic spine(S), Mitochondria(M) and postsynaptic density (white arrow) . Scale bar, 0.5 μm.

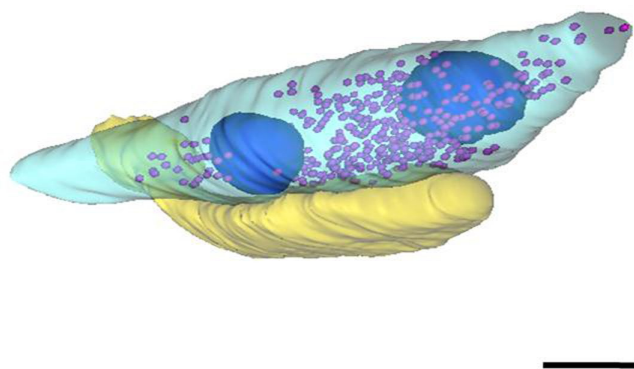


Fig. 3. Three-dimensional reconstruction of axospinous synapses from cerebellar purkinje fibers showing: Single spine bouton.. AV (turquoise color), SV (purple), Mit. (blue), S (yellow). Scale bar, 0.5μm.

synaptic axonal varicosity. It has been observed that, each synaptic vesicle appeared 4-5 times in serial images. Results showed that the number of synaptic vesicles was variable. The synaptic vesicles arranged in three groups docked, proximal and distal vesicles. The docked vesicles was attached to the presynaptic membrane, the proximal vesicles were less than two vesicle diameters from the presynaptic membrane and the distal vesicles were located more than two vesicles diameter from the presyn

aptic membrane (Fig. 4).

The number of synaptic vesicles ranged from 59-392. The average number was 171.55 ± 19.5462 vesicles per varicosity (Table 2).

The density of synaptic vesicles was variable between different varicosities.

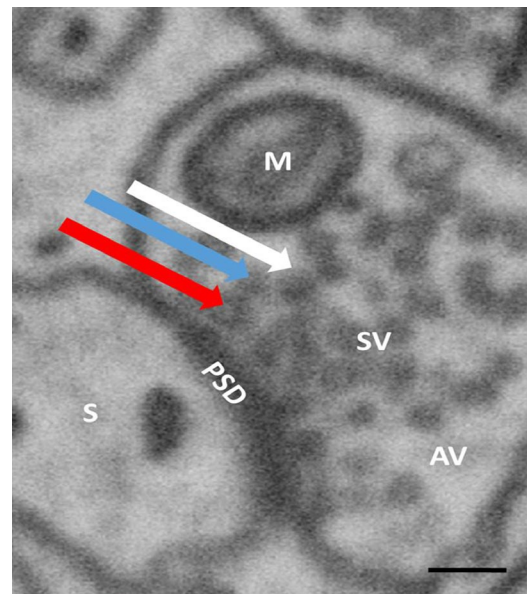


Fig. 4. Axospinous synapse from mouse cerebellum purkinje fibers showing: Synaptic vesicles pools. Red arrow representing the docked vesicles, blue one representing proximal vesicles and the white one representing distal vesicles. Axonal varicosity(AV), Synaptic vesicles (SV), Mitochondria (M), Spine (S) and Postsynaptic density (PSD). Scale bar, 200 nm.

Mitochondria

The mitochondria in presynaptic axonal varicosities were unevenly distributed. Some of presynaptic axonal varicosities had one mitochondrion and some had more than one.

From the reconstructed axospinous synapses, more than half of these synapses had mitochondria. The mitochondria present in about 65% (13/20) from the reconstructed varicosities.

The volume of mitochondria ranged from 0.017 - 0.098 mm³ with average volume of 0.050 ± 0.0072 mm³ (Table 2).

Postsynaptic compartment

Dendritic spine

The dendritic spines showed high diversity in shapes and size within the same synaptic connection and in between different synaptic populations. These diversity was clearly shown with the

three dimensional reconstructions. Different shapes, thin and mushroom shaped spines were distinguished. Most dendritic spines of cerebellar purkinje fibers were thin with macular postsynaptic density. The dendritic spine had a large voluminous head and narrow short neck (Fig. 5).

The number of spines connected to the presynaptic varicosity was varied, it commonly one dendritic spine / varicosity and 5% from the reconstructed synapses were connected with two dendritic spines (Fig. 2).

The volume of dendritic spines ranged from 0.126 - 0.264 mm³ with an average volume of 0.168 ± 0.0064 mm³ (Table 3).

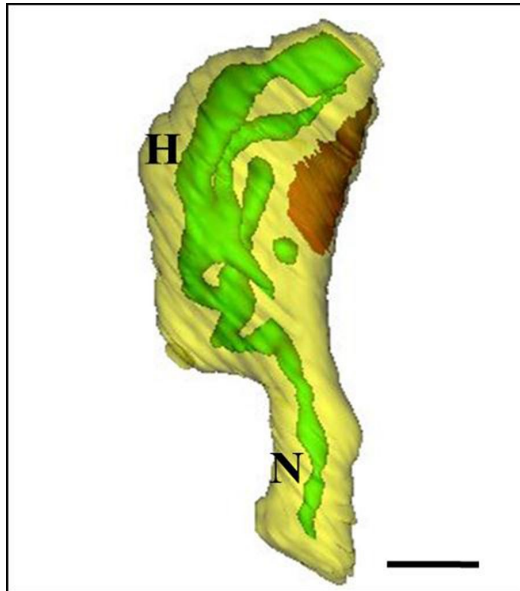


Fig. 5. Three-dimensional reconstruction of dendritic spines from different regions of mouse cerebellar purkinje fibers: Spine (yellow), PSD (red) and SA (green). (H) represents spine head and (N) is the spine neck. Scale bar, 0.2µm.

Postsynaptic density

The area of postsynaptic density was precisely reconstructed and measured for each synaptic contact. The area of PSD was variable in shape according to the shape of dendritic spines. Some of the reconstructed synapses had macular or perforated postsynaptic density. Actually, most of thin spines had a macular postsynaptic density which characterized by a continuous surface when viewed through serial sections (Figs. 2,4) , while larger or mushroom shaped spines had perforated postsynaptic density (Fig. 6).

The area of postsynaptic density ranged from 0.110 - 0.568 mm². The average value of the area of postsynaptic density was 0.227±0.0226 mm² (Table 3).

Smooth endoplasmic reticulum (SER) and spine apparatus (SA)

From our three-dimensional reconstruction, the tubules of smooth endoplasmic reticulum either ended in a tubule or traversed the neck up into the spine head and ended in a tubule, one or more smooth vesicles, or flat cistern. In some cases, the cisterns or tubules of smooth endoplasmic reticulum were laminated with inner and outer dense plates to form the spine apparatus. This spine apparatus usually elaborated from a single narrow tubule of SER that then branched to form two or more cisterns during its course along the neck or into the spine head. The large spines containing a spine apparatus had perforated PSDs (Fig. 1).

The smooth endoplasmic reticulum and spine apparatus pre-

sented in about 100% from the reconstructed spines .

The volume of SER and SA ranged from 0.0129 - 0.0217mm³. The average volume of smooth endoplasmic reticulum and spine apparatus was 0.0172±0.00049 mm³ (Table 3).

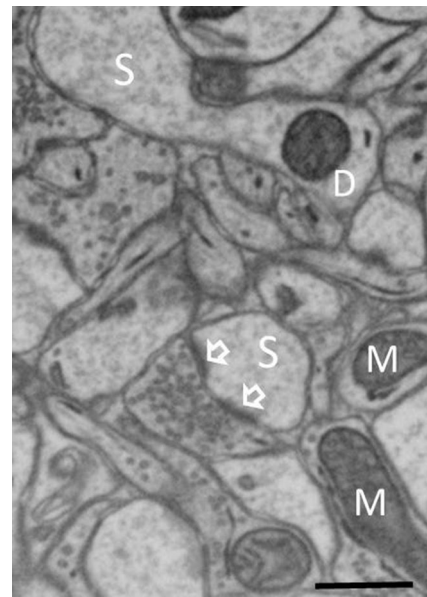


Fig. 6. Electron micrograph of the axospinous synapses from purkinje fibers of the mouse cerebellum obtained by FIB/SEM showing: Arrows represent perforated postsynaptic density, Dendritic spine (S) and Mitochondria (M). Scale bar, 0.5 µm.

Correlation analysis

Correlation between presynaptic compartments

As mentioned before, the presynaptic compartment had the presynaptic varicosity which filled with the key elements of synaptic transmission, the synaptic vesicles which bears neurotransmitters and the mitochondria. In general, the volume of presynaptic varicosity was correlated with the number of synaptic vesicles and also with the volume of mitochondria.

In synaptic connection of cerebellum, we detected a significant positive correlation between the volumes presynaptic and the number of synaptic vesicles within where, $r = 0.661^{**}$; $P = 0.001$ (Fig. 7).

The volume of presynaptic varicosity had also a significant positive correlation with the volume of mitochondria if found. It was, $r = 0.743^{**}$; $P < 0.001$ (Fig. 8).

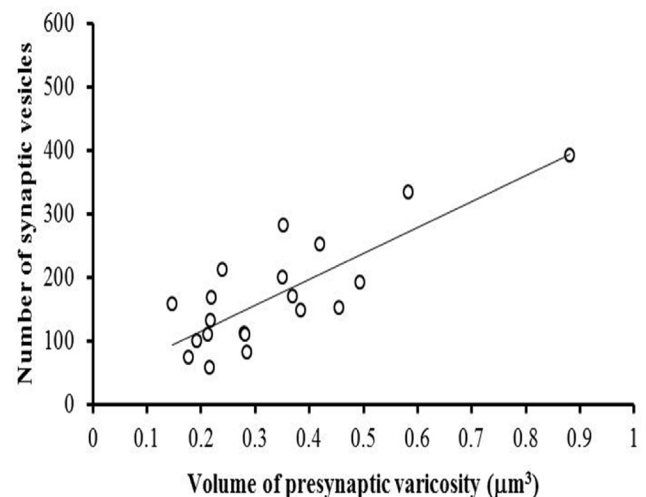


Fig. 7. Correlation between presynaptic parameters of axospinous synapses of mouse cerebellum. Scattered plot comparing the volume of presynaptic varicosities with their corresponding synaptic vesicles. The line indicating the linear regression with a correlation coefficient (r) of 0.661**.

Table 3. Summary of measurement results of post synaptic parameters.

| Postsynaptic parameters | | Cerebellum |
|-------------------------|---------------------|------------------|
| Sp | N | 21 |
| | V (range) | 0.126 - 0.264 |
| | V (average) ± SE | 0.168 ± 0.0064 |
| PSD | N | 21 |
| | Apsd (range) | 0.110 - 0.568 |
| | Apsd (average) ± SE | 0.227 ± 0.0226 |
| sER&SA | N | 21 |
| | V (range) | 0.0129 - 0.0217 |
| | V (average) ± SE | 0.0172 ± 0.00049 |

N (Number), V (Volume), SE (Standard Error).

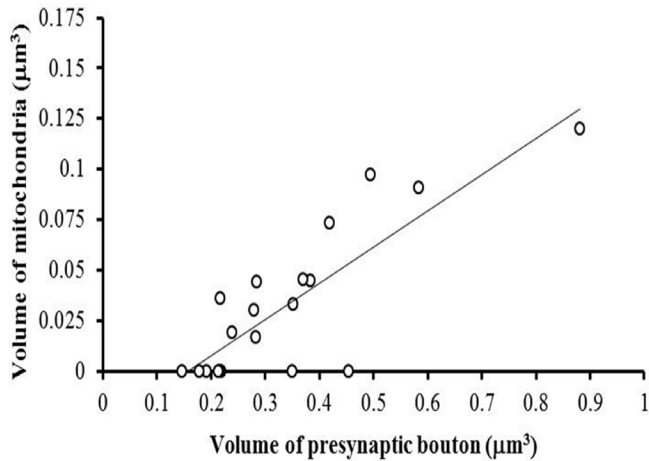


Fig. 8. Correlation between presynaptic parameters of axospinous synapses of mouse cerebellum. Scattered plot comparing the volume of presynaptic varicosities with the volume of mitochondria. The line indicating the linear regression with a correlation coefficient (r) of 0.743**.

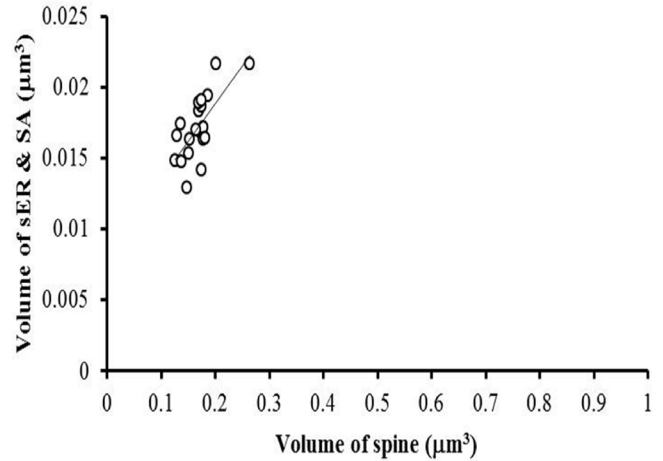


Fig. 10. Correlation between postsynaptic parameters of axospinous synapses of mouse cerebellum. Scattered plot comparing the volume of dendritic spine with the volume of smooth endoplasmic reticulum and spine apparatus. The line indicating the linear regression with a correlation coefficient (r) of 0.578**.

Correlation between postsynaptic compartments

The present study revealed that each dendritic spine was correlated with its corresponding postsynaptic density and also with smooth endoplasmic reticulum or spine apparatus if found.

We could find a significant positive correlation between the volume of dendritic spine and the area of postsynaptic density. This correlation was, $r = 0.619^{**}$; $P = 0.003$ (Fig. 9).

The volume of smooth endoplasmic reticulum was significantly correlated with the corresponding dendritic spine. It was, $r = 0.578^{**}$; $P = 0.006$ (Fig. 10).

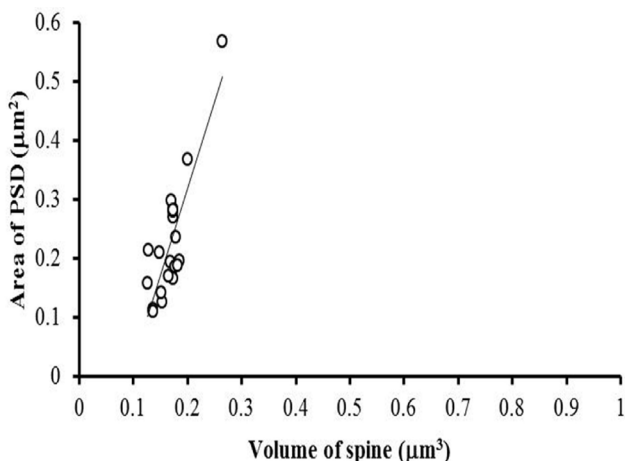


Fig. 9. Correlation between postsynaptic parameters of axospinous synapses of mouse cerebellum. Scattered plot comparing the volume of dendritic spine with the area of postsynaptic density. The line indicating the linear regression with a correlation coefficient (r) of 0.619**.

Correlation between presynaptic and postsynaptic compartments

Novel correlations were found between presynaptic and postsynaptic parameters. These results revealed the presence of significant positive correlation between the volume of presynaptic varicosity and the total volume of spine. Moreover the volume of presynaptic varicosity was significantly correlated with the total area of postsynaptic densities.

Surprising correlations were detected between the number of synaptic vesicles within the axonal varicosity and the total volume of spine and the total area of postsynaptic density.

We correlated pre and postsynaptic parameters in cerebellum. A significant positive correlation was detected between the the volume of presynaptic axonal varicosities and the total volume of spines. It was $r = 0.743^{**}$; $P < 0.001$ (Fig. 11). also, significant correlation was found between the total volume of spine and the number of synaptic vesicles. It was, $r = 0.429$; $P = 0.059$ (Fig. 12). Moreover, a significant positive correlation was detected between the volume of presynaptic varicosities and the total area of postsynaptic density which was $r = 0.644^{**}$; $p = 0.002$ (Fig. 13).

We also found that the the number of synaptic vesicles was significantly correlated with the total area of postsynaptic density, it was $r = 0.660^{**}$; $p = 0.002$ (Fig. 14).

DISCUSSION

Delineating the structure and the molecular composition of axospinous synapses is a crucial step to understand the mechanisms underlying synaptic transmission and the effective modulation of transmission connected with short and long term synaptic

plasticity (Harris and Weinberg, 2012).

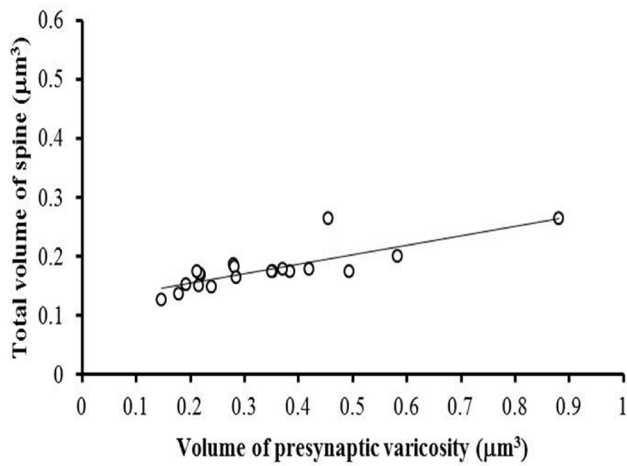


Fig. 11. Correlation between presynaptic and postsynaptic parameters of axospinous synapses parameters of axospinous synapses of mouse cerebellum. Scatter plot comparing the volume of presynaptic varicosities with their corresponding total volume of dendritic spines. The line indicating the linear regression with a correlation coefficient (r) of 0.743**.

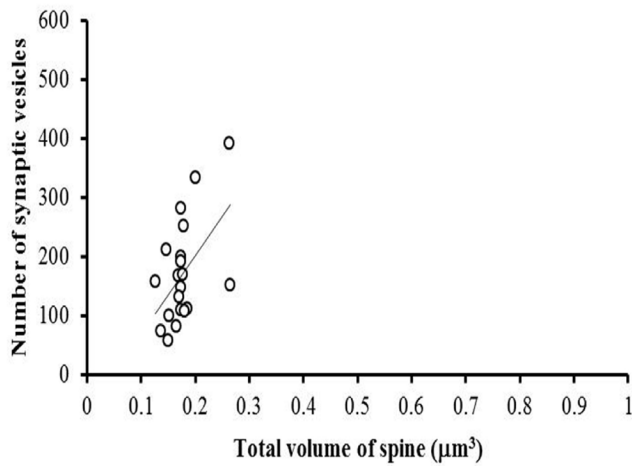


Fig. 12. Correlation between presynaptic and postsynaptic parameters of axospinous synapses parameters of axospinous synapses of mouse cerebellum. Scatter plot comparing the total volume of spines with the number of synaptic vesicles within the corresponding dendritic spines. The line indicating the linear regression with a correlation coefficient (r) of 0.429.

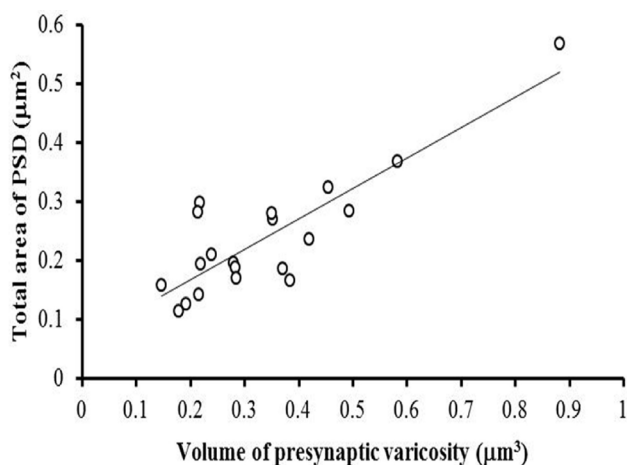


Fig. 13. Correlation between presynaptic and postsynaptic parameters of axospinous synapses parameters of axospinous synapses of mouse cerebellum. Scatter plot comparing the volume of presynaptic varicosities with their corresponding total areas of postsynaptic densities. The line indicating the linear regression with a correlation coefficient r= 0.644**.

In the present study, most of reconstructed axonal varicosities had only one spine synapsing with them (single spine bouton SSB). Some varicosities had more than one spine synapsing with them (multispine bouton MSB) and the frequency of MSB was 5%.

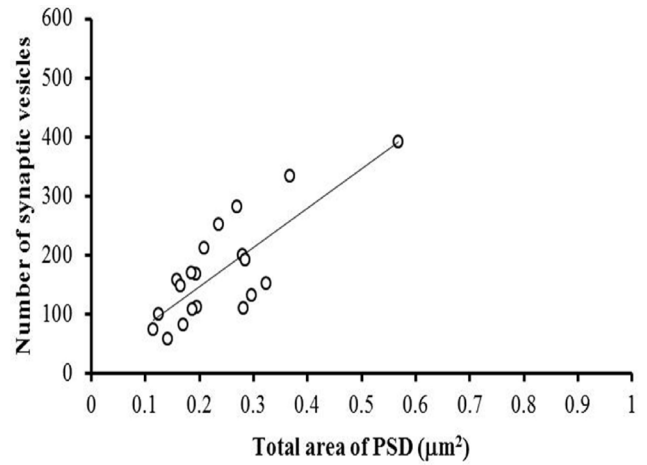


Fig. 14. Correlation between presynaptic and postsynaptic parameters of axospinous synapses parameters of axospinous synapses of mouse cerebellum. Scatter plot comparing the total area of postsynaptic density with the number of synaptic vesicles. The line indicating the linear regression with a correlation coefficient r= 0.660**.

This study revealed that individual synaptic vesicle became easily and accurately identified and counted by FIB/SEM with 10 nm Z-step. Each vesicle can be seen from 4 to 5 times in serial images. This method overcomes the ambiguous identification of synaptic vesicles using ssTEM due to the thickness of sections (60 nm) and density of staining as mentioned by Bartol *et al.* (2015).

The current investigation indicated that the number of synaptic vesicles is variable and arranged in three groups; docked (readily releasable pool), proximal (recycling pool) and distal vesicles (reserve pool). The docked vesicles found attached to the presynaptic membrane, the proximal vesicles were less than two vesicle diameters from the presynaptic membrane and the distal vesicles were located more than two vesicles diameter from the presynaptic membrane. Rosenmund *et al.* (2003) added that excitatory presynaptic boutons contain clear round vesicles, approximately 35-50 nm in diameter. These vesicles usually contain the neurotransmitter glutamate. Exocytosis of neurotransmitters requires the docking and fusion of vesicles with the plasma membrane and requires ATP and voltage-gated calcium channels. Moreover, Haucke *et al.* (2011) added that the synaptic vesicles can be separated into three pools by function and location within the presynaptic terminal: the readily-releasable pool (RRP), the recycling pool, and the reserve pool. SVs in the RRP are available for immediate exocytosis upon Ca_2^+ entry, being both docked and primed, but in the classical model this pool accounts for only ~1-2% of total SVs and is rapidly depleted during high-frequency stimulation. Rizzoli and Betz (2005) suggested that the recycling pool is necessary for the continuation of moderate (physiological) levels of stimulation and is believed to contain ~10-20% of the total SVs. Lastly; the reserve pool is the largest pool, believed to contain ~80-90% of the total SVs.

Results obtained in this work indicated that the number of synaptic vesicles is variable in each synaptic varicosity, where it ranged from 59-392. The average number was 171.55 ± 19.5462 vesicles per varicosity.

Elhanbaly (2017) recorded that the number of synaptic vesicles in the hippocampus of wild type mouse were ranged from 67-268, 9-226, 12-144 and 53-501 vesicles per bouton in DG-mml1, DG-oml, CA1-sr and CA1-sl respectively. The average number was 159.0 ± 14.53 , 118 ± 15.10 , 52.0 ± 9.06 and 167.1 ± 23.10 vesicles per bouton in DG-mml1, DG-oml, CA1-sr and CA1-sl respectively.

Harris and Kater (1994) stated that the typical presynaptic terminal may contain a few hundred synaptic vesicles, although this number varies widely among synapses. Moreover, Schikorski and Stevens (1997) reported that by using three-dimensional reconstructions of CA1 excitatory synapses in the rodent hippocampus and in culture, the number of docked vesicles per active zone was ~10, and the total number of vesicles per bouton was 270 with a range from 40 to 801.

According to the obtained results, the mitochondria in pre-

synaptic axonal varicosities were unevenly distributed. Some of presynaptic axonal varicosities had one mitochondrion and some had more than one. synapses had mitochondria. The mitochondria presented in about 65% (13/20) from the reconstructed varicosities. The volume of mitochondria ranged from 0.017 - 0.098 mm³ with average volume of 0.050 ± 0.0072 mm³

Elhanbaly (2017) recorded that the mitochondria presented in about 45%, 35%, 35% and 30% from the reconstructed varicosities in DG-mml1, DG-oml, CA1-sl and CA1-sr of hippocampus.

In agreement with Nafstad and Blackstad (1966), the mitochondria are unevenly distributed in axons, as they are elsewhere in the CA1 neuropil. They added that mitochondria occur in less than 50% of synaptic boutons. This finding raises several questions regarding energy use and calcium regulation, especially during synaptic activation. Furthermore, Shepherd and Harris (1998) reported that the mitochondria are distributed heterogeneously along axons and in the presynaptic boutons where only 41% of presynaptic boutons contain mitochondria in the hippocampal CA1.

Regarding to the function of mitochondria within axospinous synapses, Sheng (2014) stated that the mitochondria are essential organelles for neuronal growth, survival, and function. Neurons use specialized mechanisms to drive mitochondria transport and to anchor them in axons and at synapses. Stationary mitochondria buffer intracellular Ca₂⁺ and serve as a local energy source by supplying ATP. The balance between motile and stationary mitochondria responds quickly to changes in axonal and synaptic physiology. Defects in mitochondrial transport and distribution are implicated in the pathogenesis of several major neurological disorders.

The present findings indicated a significant positive correlation between the volume of presynaptic varicosities and the number of synaptic vesicles as well as with the volumes of mitochondria in all studied hippocampal regions even in sept3 KO mouse.

In agreement with Harris *et al.* (1992) the volume of presynaptic varicosities is correlated well with its corresponding number of synaptic vesicles and mitochondria in CA1-sr region of mouse hippocampus.

The dendritic spines in this study showed high diversity in shapes and size within the same synaptic connection. This diversity is clearly shown with the three dimensional reconstructions of dendritic spines. Tashiro and Yuste (2003) added that spine morphology is very diverse and spine size is correlated with the strength of the synaptic transmission. Also, the spine neck biochemically isolates individual synapses. Therefore, spine morphology directly reflects its function.

Adrian *et al.* (2014) mentioned that the dendritic spines are micron-sized protrusions that harbor the majority of excitatory synapses in the central nervous system. The head of the spine is connected to the dendritic shaft by a 50-400 nm thin membrane tube, called the spine neck, which has been hypothesized to confine biochemical and electric signals within the spine compartment. Such compartmentalization could minimize intersynaptic crosstalk and thereby support spine-specific synapse plasticity.

The dendritic spine has a large voluminous head and narrow short neck. Nieto-Sampedro *et al.* (1982) added that the molecular layer of the dentate gyrus of normal rats shows a large incidence of perforated postsynaptic densities (PSDs). The perforations or discontinuities occur almost exclusively in PSDs located in spines showing a U- or W-shaped junctional profile (complex PSDs). In relation to that point, Matsuzaki *et al.* (2001) and Kasai *et al.* (2003) mentioned that the dendritic spines, which receive most of the excitatory synaptic input in the cerebral cortex, are heterogeneous with regard to their structure, stability and function. Spines with large heads are stable, express large numbers of AMPA-type glutamate receptors, and contribute to strong synaptic connections. By contrast, spines with small heads are motile and unstable and contribute to weak or silent synaptic connections. Their structure-stability-function relationships suggest that large and small spines are memory spines and learning

spines respectively. Given that turnover of glutamate receptors is rapid, spine structure and the underlying organization of the actin cytoskeleton are likely to be major determinants of fast synaptic transmission and, therefore, are likely to provide a physical basis for memory in cortical neuronal networks. The distribution of functional AMPA receptors is tightly correlated with spine geometry and that receptor activity is independently regulated at the level of single spines.

Regarding to the function of spines, Swindale (1981) mentioned that one possible function of dendritic spines is the increase of the surface area of dendrites and thus the number of possible synapses per dendritic length. Bonhoeffer and Yuste (2002) added that the spines allow dendrites to reach multiple axons, minimizing the distances from one synapse to the next. Tao-Cheng *et al.* (2001) added that alterations in spine organelles result from diverse causes. One cause may be degeneration of the postsynaptic cell, as is often the case when the dendritic cytoplasm becomes dense and dark. Another cause may be excitotoxic injury from excessive presynaptic glutamate release, which characteristically leads to thickening of the postsynaptic density, a condition often seen in ischemia. Ischemia also induces postsynaptic density-like structures that lie free in the cytoplasm of the dendrite.

Cruz-Martin *et al.* (2010) and Portera-Cailliau (2012) illustrated that many pathological conditions lead to changes in the number of dendritic spines along spiny dendrites. Spine loss commonly occurs within a few days of differentiation. Permanent spine loss is evident in most forms of mental retardation, including those resulting from prenatal infection, malnutrition, and toxin or alcohol exposure. Spine loss is also seen in epilepsy, prionosis and various neurodegenerative disorders. Increased spine density is seen paradoxically in some types of differentiation, such as when Purkinje cells are deprived of their climbing fiber input. Increased spine numbers have also been reported following chronic use of stimulatory drugs. In some cases, an overabundance of dendritic spines may represent a failure of normal developmental synapse elimination, as has been suggested for fragile-X syndrome

The present study revealed that the postsynaptic density within dendritic spines emerges in two morphologically distinguished forms. The macular PSD which mostly found in thin spines and characterized by continuous electron dense thickness when viewed through serial sections on spine head and perforated one, mostly presented in large mushroom shaped spines.

In agreement with Magee and Johnston (2005) the surfaces of the PSDs vary from small discs to large irregular shapes that can be perforated by electron lucent regions. Moreover, Nicholson *et al.* (2006) suggested that differences in PSD dimensions can reflect distance-dependent differences in dendritic function. Relatively more of the distal synapses on CA1 pyramidal cells have perforated synapses; however, perforated synapses associated with the distal input of entorhinal cortex host a lower density of AMPA receptors than perforated synapses at proximal CA3 input of the same CA1 cells. Geinisman *et al.* (1991); Toni *et al.* (1999); Dhanrajan *et al.* (2004) and Popov *et al.* (2004) added that PSDs appear larger and are more likely to have perforations shortly after the induction of LTP; consistent with the idea that perforations are transient structural perturbations responding to activation (Lisman and Harris, 1994; Fiala *et al.*, 2002; Spacek and Harris, 2004). Larger spines with more AMPA and NMDA receptors in the PSD are more sensitive to glutamate (Takumi *et al.*, 1999a; Takumi *et al.*, 1999b; Matsuzaki *et al.*, 2001). While small spine synapses only contain NMDA receptors (Liao *et al.*, 1995; Liao *et al.*, 1999; Petralia *et al.*, 1999; Park *et al.*, 2004; Kopec *et al.*, 2006). AMPA receptors must be constitutively exchanged to sustain the newly active spines; fortunately, lateral diffusion of AMPA receptors out of a spine is limited by the constricted spine neck (Ashby *et al.*, 2006).

This study indicated that the volume of dendritic spine is significantly correlated with corresponding area of postsynaptic density as well as with the volume of smooth endoplasmic reticulum and spine apparatus. In accordance with Harris and Ste-

vens (1989) as well as Harris *et al.* (1992), the spine volume is well correlated with postsynaptic density and smooth endoplasmic reticulum of CA1-sr of mouse hippocampus. There is likely a trans-synaptic mechanism to coordinate them during plasticity (Spacek and Harris, 2004).

In the present work, the tubules of smooth endoplasmic reticulum either end in a tubule or traverse the neck up into the spine head and ended in a tubule, one or more smooth vesicles, or flat cistern. In some cases, the cisterns or tubules of smooth endoplasmic reticulum are laminated with inner and outer dense plates to form the spine apparatus. This spine apparatus usually elaborated from a single narrow tubule of SER that then branched to form two or more cisterns during its course along the neck or into the spine head. The large spines containing a spine apparatus had perforated PSDs. As in other brain regions, the spine apparatus in the hippocampal area CA1 appeared in the large dendritic spines that possessed perforated postsynaptic densities and is absent in small spines with macular postsynaptic densities similar to that observed by Spacek and Harris (1997).

Related to the function of smooth endoplasmic reticulum, Ghadially (1982) mentioned that the rough endoplasmic reticulum is prominent in the nerve cell body and proximal dendrites, whereas in the distal parts of dendrites and dendritic spines the smooth endoplasmic reticulum predominates. He added that the smooth endoplasmic reticulum in various cells of different tissues is thought to play important roles in the regulation of chloride ions; in the transport of lipids and circulation of membrane phospholipids and glycoproteins; in the metabolism of lipids, lipoproteins and glycogen; in the synthesis of steroid hormones and in detoxification.

A significant correlation between the dimensions of SER and the dimensions of dendritic spines or synapses size in cerebellum and visual cortex (Harris and Stevens, 1988). Same correlation was obtained by studying the SER of the hippocampal area CA1 of mouse hippocampus (Spacek and Harris, 1997).

Spacek and Harris (1997) mentioned that there are high levels of calcium in activated dendritic spines, where the smooth endoplasmic reticulum is likely to be important for regulating calcium. They measured the dimensions and organization of the SER in hippocampal spines and dendrites through serial electron microscopy and three-dimensional analysis. SER of some form is found in 58% of the immature spines and in 48% of the adult spines. Less than 50% of the small spines at either age contained SER, suggesting that other mechanisms, such as cytoplasmic buffers, regulate ion fluxes within their small volumes. In contrast, 80% of the large mushroom spines of the adult had a spine apparatus, an organelle containing stacks of SER and dense-staining plates.

The present study confirmed that the focused ion beam scanning electron microscopy is a powerful tool for accurate identification of synaptic macro and microelements.

CONCLUSION

Axospinous synapses are excitatory synaptic contacts established on dendritic spines, small protrusions that extend from dendrites of postsynaptic neurons. These synapses are normally consisted of mitochondria, synaptic vesicles and an active zone in a presynaptic axonal varicosity and a postsynaptic density and smooth endoplasmic reticula (spine apparatuses) in a spine. It is important to discriminate between normal organization and various anomalies of axospinous synapses. However, fine morphological investigation of these synapses is often hampered by low spatial resolution in z-axis (> 40 nm) and distortion of ultrastructure in conventional transmission electron microscopy.

CONFLICT OF INTEREST

The authors declare that they have no conflict of interest.

REFERENCES

- Adrian, M., Kusters, R., Wierenga, C.J., Storm, C., Hoogenraad, C.C., Kapitein, L.C., 2014. Barriers in the brain: Resolving dendritic spine morphology and compartmentalization. *Frontier of Neuroanatomy* 8, 1-12.
- Arellano, J.I., Benavides-Piccione, R., Defelipe, I., Yuste, R., 2007. Ultrastructure of dendritic spines: correlation between synaptic and spine morphologies. *Frontier of Neuroscience* 1, 131-143.
- Ashby, M.C., Maier, S.R., Nishimune, A., Henley, J.M., 2006. Lateral diffusion drives constitutive exchange of AMPA receptors at dendritic spines and is regulated by spine morphology. *Journal of Neuroscience* 26, 7046-7055.
- Bartol, T.M., Bromer, C., Kinney, J., Chirillo, M.A., Bourne, J.N., Harris, K.M., Sejnowski, T.J., 2015. Nanoconnectomic upper bound on the variability of synaptic plasticity *Elife*, 1-18.
- Bonhoeffer, T., Yuste, R., 2002. Spine motility. Phenomenology, mechanisms and function. *Neuron* 35, 1019-1027.
- Burns, M.E., Augustine, G.J., 1995. Synaptic structure and function: dynamic organization yields architectural precision. *Cell* 83, 187-194.
- Cruz-Martin, A., Crespo, M., Portera-Cailliau, C., 2010. Delayed stabilization of dendritic spines in fragile K mice. *Journal of Neuroscience* 30, 7793-7803.
- DeFelipe, J., 2009. The neuroanatomist's dream, the problems and solutions and the ultimate aim. *Frontier Neuroscience* 2, 10-12.
- Dhanraj, T.M., Lynch, M.A., Kelly, A., Popov, V.I., Rusakov, D.A., Stewart, M.G., 2004. Expression of long-term potentiation in aged rats involves perforated synapses but dendritic spine branching results from high frequency stimulation alone. *Hippocampus* 14, 255-264.
- Elhanbaly, R., 2017. Studies on morphological and molecular characteristics of neuronal networks responsible for learning and memory. Ph. D thesis, Assiut University, Egypt.
- Fiala, J.C., Spacek, J., Harris, K.M., 2002. Dendritic spine pathology: cause or consequence of neurological disorders?. *Brain Research Review* 39, 29-54.
- Geinisman, Y., Toledo-Morrell, L., Morrell, F., 1991. Induction of long-term potentiation is associated with an increase in the number of axospinous synapses with segmented postsynaptic densities. *Brain Research* 566, 77-88.
- Ghadially, F.N., 1982. Ultrastructure pathology of the cell. London: Butterworths.
- Harris, K.M., Kater, S.B., 1994. Dendritic spines: Cellular specializations imparting both stability and flexibility to synaptic function. *Annals Review Neuroscience* 17, 341-371.
- Harris, K.M., Stevens, J.K., 1988. Dendritic spines of rat cerebellar Purkinje cells: Serial electron microscopy with reference to their biophysical characteristics. *Journal of Neuroscience* 8, 4455-4469.
- Harris, K.M., Stevens, J.K., 1989. Dendritic spines of CA1 pyramidal cells in the rat hippocampus: Serial electron microscopy with reference to their biophysical characteristics. *Journal of Neuroscience* 9, 2982-2997.
- Harris, K.M., Weinberg, R.J., 2012. Ultrastructure of synapses in the mammalian brain. *Cold Spring Harb. Perspective Biology* 4, 1-30.
- Harris, K.M., Jensen, F.E., Tsao, B., 1992. Three-dimensional structure of dendritic spines and synapses in rat hippocampus (CA1) in postnatal day 15 and adult ages: Implications for the maturation of synaptic physiology and long-term potentiation. *Journal of Neuroscience* 12, 2685-2705.
- Harris, K.M., Perry, E., Bourne, J., Feinberg, M., 2006. Uniform serial sectioning for transmission electron microscopy. *Journal of Neuroscience* 26, 12101-12103.
- Hauke, V., Neher, E., Sigris, S.J., 2011. Protein scaffolds in the coupling of synaptic exocytosis and endocytosis. *Nature Review Neuroscience* 12, 127-138.
- Hoffpauir, B.K., Pope, B.A., Spirou, G.A., 2007. Serial sectioning and electron microscopy of large tissue volumes for 3D analysis and reconstruction: a case study of the calyx of Held. *Nature Protection* 2, 9-22.
- Kasai, H., Matsuzaki, M., Noguchi, J., Yasumatsu, N., Nakahara, H., 2003. Structure-stability-function relationships of dendritic spines. *Trends in Neuroscience* 26, 360-368.
- Knott, G., Rosset, S., Cantoni, M., 2011. Focussed ion beam milling and scanning electron microscopy of brain tissue. *Journal of Visualized Experiments* 6, 2588.
- Kopec, C.D., Li, B., Wei, W., Boehm, J., Malinow, R., 2006. Glutamate receptor exocytosis and spine enlargement during chemically induced long-term potentiation. *Journal of Neuroscience* 26, 2000-2009.
- Kubota, Y., Hatada, S.N., Kawaguchi, Y., 2009. Important factors for the three-dimensional reconstruction of neuronal structures from se-

- rial ultrathin sections. *Frontier Neural Circuits* 3, 1-10.
- Liao, D., Hessler, N.A., Malinow, R., 1995. Activation of postsynaptically silent synapses during pairing-induced LTP in CA1 region of hippocampal slice. *Nature* 375, 400-404.
- Liao, D. X. Zhang, Brien, R., Ehlers, M.D., Hugarir, R.L., 1999. Regulation of morphological postsynaptic silent synapses in developing hippocampal neurons. *Nature Neuroscience* 2, 37-43.
- Lishman, J., Harris, K.M., 1994. Who's been nibbling on my PSD: Is it LTD? *Journal of Physiology (Paris)* 88,193-195.
- Magee, J.C., Johnston, D., 2005. Plasticity of dendritic function. *Current Opinion Neurobiology* 15, 334-342.
- Matsuzaki, M., Ellis-Davies, G.C.R., Nemoto, T., Miyashita, Y., Iino, M., Haruo, K., 2001. Dendritic spine geometry is critical for AMPA receptor expression in hippocampal CA1 pyramidal neurons. *Nature Neuroscience* 4, 1086-1092.
- Merchan-Perez, A., Rodriguez, J.R., Alonso-Nanclares, L., Andreas, S., Defelipe, J., 2009. Counting synapses using FIB/SEM microscopy: a true revolution for ultrastructural volume reconstruction. *Frontier Neuroanatomy* 3, 1-14.
- Nafstad, H.J., Blackstad, T.W., 1966. Distribution of mitochondria in pyramidal cells and boutons in hippocampal cortex. *Z Zellforsch Mikrosk. Anatomy* 73, 234-245.
- Nicholson, D.A., Trana, R., Katz, Y., Kath, W.L., Spruston, N., Geinisman, Y., 2006. Distance-dependent differences in synapse number and AMPA receptor expression in hippocampal CA1 pyramidal neurons. *Neuron* 50, 431-442.
- Park, M., Penick, E.C., Edwards, J.G., Kauer, J.A., Ehlers, M.D., 2004. Recycling endosomes supply AMPA receptors for LTP. *Science* 305, 1972-1975.
- Petralia, R.S., Esteban, J.A., Wang, Y.X., Partridge, J.G., Zhao, H.M., 1999. Selective acquisition of AMPA receptors over postnatal development suggests a molecular basis for silent synapses. *Nature Neuroscience* 2, 31-36.
- Popov, V.I., Davies, H.A., Rogachevsky, V.V., Patrushev, I.V., Errington, M.L., 2004. Remodelling of synaptic morphology but unchanged synaptic density during late phase long-term potentiation (LTP): a serial section electron micrograph study in the dentate gyrus in the anaesthetised rat. *Neuroscience* 128, 251-262.
- Portera-Cailliau, C., 2012. Which comes first in fragile X syndrome, dendritic spine dysgenesis or defects in circuit plasticity?. *Neuroscientist* 18, 28-44.
- Rizzoli, S.O., Betz, W.J., 2004. The structural organization of the readily releasable pool of synaptic vesicles. *Science* 303, 2037-2039.
- Rizzoli, S.O., Betz, W.J., 2005. Synaptic vesicles pools. *Nature Review Neuroscience* 6, 57-69.
- Rollenhagen, A., Lübke, J.H.R., 2006. The morphology of excitatory central synapses: from structure to function. *Cell Tissue Research* 326, 221-237.
- Rosenmund, C., Rettig, J., Brose, N., 2003. Molecular mechanisms of active zone function. *Current Opinion Neurobiology* 13, 509-519.
- Schikorski, T., Stevens, C.F., 1997. Quantitative ultrastructural analysis of hippocampal excitatory synapses. *Journal of Neuroscience* 17, 5858-5867.
- Sheng, Z., 2014. Mitochondrial trafficking and anchoring in neurons: New insight and implications. *Journal of Cell Biology* 204, 1087-1098.
- Spacek, J., Harris, K.M., 1997. Three-dimensional organization of smooth endoplasmic reticulum in hippocampal CA1 dendrites and dendritic spines of the immature and mature rat. *Journal of Neuroscience* 17, 190-203.
- Spacek, J., Harris, K.M., 2004. Trans-endocytosis via spinules in adult rat hippocampus. *Journal of Neuroscience* 24, 4233-4241.
- Swindale, N., 1981. Dendritic spines only connect. *Trends Neurosci.* 4, 240-241.
- Takumi, Y., Matsubara, A., Rinvik, E., Ottersen, O.P., 1999a. The arrangement of glutamate receptors in excitatory synapses. *Ann. N Y Acad. Sci.* 868, 474-482.
- Takumi, Y., Ramirez-Leon, V., Laake, P., Rinvik, E., Ottersen, O.P., 1999b. Different modes of expression of AMPA and NMDA receptors in hippocampal synapses. *Nature Neuroscience* 2, 618-624.
- Tao-Cheng, J.H., Vinade, L., Smith, C., Winters, C.A., Ward, R., Brightman, M.W., Reese, T.S., Dosemeci, A., 2001. Sustained elevation of calcium induces Ca²⁺/calmodulin-dependent protein kinase II clusters in hippocampal neurons. *Neuroscience* 106, 69-78.
- Tashiro, A., Yuste, R., 2003. Structure and molecular organization of dendritic spines. *Histology & Histopathology* 18, 617-634.
- Toni, N., Buchs, P.A., Nikonenko, I., Bron, C.R., Muller, D., 1999. LTP promotes formation of multiple spine synapses between a single axon terminal and a dendrite. *Nature* 402, 421-425.